catalysts

MDPI

Article

FeCo Alloy-Decorated Proton-Conducting Perovskite Oxide as an Efficient and Low-Cost Ammonia Decomposition Catalyst

Xueyan Zhao [1,2], Qingfeng Teng [2], Haoliang Tao [2], Wenqiang Tang [2], Yiwei Chen [3], Bofang Zhou [3], Junkang Sang [2], Senrui Huang [2], Wanbing Guan [2], Hua Li [2,*] and Liangzhu Zhu [2,3,*]

[1] School of Materials Science and Chemical Engineering, Ningbo University, No.818 Fenghua Road, Ningbo 315211, China
[2] Zhejiang Key Laboratory of Advanced Fuel Cells and Electrolyzers Technology, Ningbo Institute of Mate Rials Technology and Engineering, Chinese Academy of Sciences, Ningbo 315201, China
[3] College of Materials Science and Engineering, Hubei University of Automotive Technology, Shiyan 442002, China
* Correspondence: li.hua.fcsl@nimte.ac.cn (H.L.); zhuliangzhu@nimte.ac.cn (L.Z.)

Abstract: Ammonia is known as an alternative hydrogen supplier because of its high hydrogen content and convenient storage and transport. Hydrogen production from ammonia decomposition also provides a source of hydrogen for fuel cells. While catalysts composed of ruthenium metal atop various support materials have proven to be effective for ammonia decomposition, non-precious-metal-based catalysts are attracting more attention due to desires to reduce costs. We prepared a series of Fe, Co, Ni, Mn, and Cu monometallic catalysts and their alloys as catalysts over proton-conducting ceramics via the impregnation method as precious-metal-free ammonia decomposition catalysts. While Co and Ni showed superior performance compared to Fe, Mn, and Cu on a $BaZr_{0.1}Ce_{0.7}Y_{0.1}Yb_{0.1}O_{3-\delta}$ (BZCYYb) support as an ammonia decomposition catalyst, the cost of Fe is much lower than that of other metals. Alloying Fe with Co can significantly increase the conversion and stability and lower the overall cost of materials. The measured ammonia decomposition rate of FeCo/BZCYYb reached 100% at 600 °C, and the ammonia decomposition rate was almost unchanged during the long-term test of 200 h, which reveals its good catalytic activity for ammonia decomposition and thermal stability. When the metallic catalyst remained unchanged, BZCYYb also exhibited better performance compared to other commonly used oxide supports. Finally, when ammonia cracked using our alloy catalyst was fed to solid oxide fuel cells (SOFCs), the peak power densities were very close to that achieved with a simulated fully cracked gas stream, i.e., 75% H_2 + 25% N_2, thus proving the effectiveness of this new type of ammonia decomposition catalyst.

Keywords: ammonia decomposition; bimetallic catalyst; solid oxide fuel cells; BZCYYb

Citation: Zhao, X.; Teng, Q.; Tao, H.; Tang, W.; Chen, Y.; Zhou, B.; Sang, J.; Huang, S.; Guan, W.; Li, H.; et al. Using FeCo Alloy-Decorated Proton-Conducting Perovskite Oxide as an Efficient and Low-Cost Ammonia Decomposition Catalyst. *Catalysts* **2024**, *14*, 850. https://doi.org/10.3390/catal14120850

Academic Editor: Bruno Fabre

Received: 24 October 2024
Revised: 18 November 2024
Accepted: 20 November 2024
Published: 23 November 2024

1. Introduction

Hydrogen is recognized as a clean energy source because of its high combustion value. Its conversion in fuel cells generates only water as a byproduct, thus promoting the "hydrogen economy" as a predominant sustainable energy system facilitating industrial development [1]. However, it is difficult to liquefy hydrogen at room temperature, and the large-scale application of hydrogen is hindered by the limitations of its storage and transportation due to its inherently low volume energy density. Other alternative sources of hydrogen energy are being investigated, including ammonia, methanol, methane, hydrous gas, and natural gas, etc. Ammonia possesses a substantial hydrogen content of 17 wt.%, which is higher than that of methanol (12.5 wt.% of hydrogen), and liquid ammonia also has a higher volumetric density of 12.9 MJ/L compared to compressed hydrogen with a bulk density of 4.5 MJ/L [2,3]. Moreover, it exhibits superior energy efficiency, as well as being carbon-free and non-polluting, making it easy to liquefy at 8.5

atmospheres at room temperature and rendering it suitable for energy storage applications. Additionally, the technology for ammonia synthesis has evolved over the last hundred years, and is now well established and widely implemented in industrial environments. Ammonia is extensively utilized as a fertilizer in agriculture, supported by well-established infrastructure that significantly reduces the costs associated with storage and transportation [4]. The combustion range of ammonia is relatively narrow, which enhances its safety profile [1]; it also produces a strongly irritating odor, which is detectable at concentrations above 1 ppm when it leaks. In addition, when properly decomposed either in situ or ex situ, cracked ammonia provides an attractive hydrogen source for fuel cells, and has already been a very active research area [5–7]. Therefore, on-site hydrogen production from ammonia is a promising source of future sustainable energy [8].

According to thermodynamic calculations, 99% ammonia conversion can be achieved at 200 °C. However, the decomposition process is primarily limited by its kinetic barriers [9]. As a result, recent research has focused on developing catalysts that can lower the activation energy of ammonia decomposition. Ru is regarded as the most efficient single-metal catalyst for ammonia decomposition [10]. Yin et al. loaded 4.8 wt.% Ru onto Al_2O_3 with water as the solvent; the ammonia conversion was 5.9% and the hydrogen production rate was 1.9 mmol $min^{-1}g^{-1}$ at 450 °C and a gas hourly space velocity (GHSV) of 30,000 mL $h^{-1}g^{-1}$ [11]. However, due to its scarcity and status as a precious metal, Ru greatly increases the overall cost of the catalyst, making it impractical for commercialization. Moreover, residual Cl^- in the $RuCl_3$ solution typically used as a precursor for Ru catalysts negatively impacts the ammonia decomposition rate. Once KCl is formed, it becomes challenging to eliminate. Therefore, it is necessary to explore inexpensive transition metals that exhibit comparable or even superior catalytic performance and high stability that can support high loadings to achieve the desired ammonia decomposition rate, such as Fe [12], Co [13], Ni [14], Mo [15], Fe-Co [16], Fe-Ni [17], Co-Mo [18], Mg-Co-Fe, etc. [19]. T.V. Choudhary et al. loaded 10 wt.% Ni onto Al_2O_3 with an ammonia conversion of 36.4% and a hydrogen production of 11.4 mmol $min^{-1}g^{-1}$ at 600 °C and a GHSV of 30,000 mL $h^{-1}g^{-1}$ [20]. Simonsen et al. loaded 10 wt.% Fe onto Al_2O_3 with an ammonia conversion of 25% at 500 °C and a GHSV of 80000 mL $h^{-1}g^{-1}$ [21]. Yin et al. used a 0.1g Fe/CNT catalyst with a loading of 4.95×10^{-4} mol g^{-1} with a hydrogen production rate of 0.65 mmol $min^{-1}g^{-1}$ at 500 °C and a GHSV of 30,000 mL $h^{-1}g^{-1}$ [22]. Lorenzut et al. loaded 10 wt.% Fe onto YSZ and the ammonia conversion was about 20% at 600 °C and a GHSV of 46,000 mL $h^{-1}g^{-1}$ [23]. In general, Fe-based catalysts have been extensively investigated, operating at high temperatures of about 800 °C, but present challenges remain in regard to their stability. Therefore, the pursuit of bimetallic catalysts is gaining momentum due to their potential to improve both catalytic activity and stability.

At moderate to low temperatures, Fe-based catalysts generally exhibit low ammonia decomposition rates and poor stability. Nevertheless, by doping with Co metal, it is possible to develop bimetallic catalysts with dual active centers, achieving both high catalytic performance and improved stability [24]. Furthermore, FeCo catalysts exhibit exceptional electrocatalytic performance in the nitrogen reduction reaction (NRR) for ammonia synthesis performance [25], making them promising candidates for facilitating ammonia synthesis and its reversible reactions. Zhang et al. loaded 5 wt.% FeCo in CNTs with an ammonia conversion of 50% at 600 °C and a GHSV of 36,000 mL $h^{-1}g^{-1}$ [16]. Sun et al. loaded 10 wt.% FeCo onto fumed SiO_2 with 100% ammonia conversion at 630 °C and a GHSV of 14,400 mL $h^{-1}g^{-1}$ [26].

In addition to active metals, the supports also have an important effect on the catalytic activity. The support material is required to have a high specific surface area in order to ensure that the catalyst is well dispersed, as well as robust thermal stability, basicity, and electrical conductivity, which promote electron transfer between the active metal and the support. Furthermore, the support can improve catalytic efficiency through

either "structural promotion" or "electronic promotion" mechanisms [10]. $BaZr_{0.1}Ce_{0.7}Y_{0.1}Yb_{0.1}O_{3-\delta}$ (BZCYYb) has gained significant attention and become a popular proton-conducting electrolyte ever since it was reported in 2009 [27–29]. It is known that for such proton-conducting electrolytes, both H_2 and H_2O can form hydroxide ions by reacting with lattice oxygen or simultaneously with the presence of oxygen vacancies. We hypothesize that this property may benefit the intermediate steps of the ammonia decomposition process. Meanwhile, barium or its oxides have shown high effectiveness for ammonia decomposition [2,30]. Lastly, since BZCYYb has now been widely used in protonic ceramic fuel cells (PCFCs), a very active research direction, the cost of using an existing material could be further decreased. Therefore, we consider BZCYYb as a potential support material.

In this study, different single metals and their alloys, particularly the FeCo binary alloy, were employed as the active metals onto a pretreated BZCYYb support. As an alkaline earth metal, Ba significantly enhances ammonia decomposition performance via electron-donating effects [14]. Additionally, it acts as a structural promoter, influencing the local atomic arrangement of Fe and Co atoms on the surface [31]. X-ray diffraction and X-ray photoelectron spectroscopy confirmed the formation of an alloy phase. Ammonia decomposition rates were investigated within the temperature range of 450–650 °C. The material was found to demonstrate great potential for industrial-scale applications, achieving a H_2 generation rate of 6.8 mmol $min^{-1}g^{-1}$ at 600 °C with the FeCo/BZCYYb catalyst. Additionally, the FeCo/BZCYYb catalyst was tested on solid oxide fuel cells (SOFCs) in order to evaluate its electrochemical performance and suitability for fuel cell applications.

2. Results and Discussion

The TG-DSC curves of BZCYYb as a support are shown in Figure 1a. BZCYYb powder was pretreated via calcination at 1000 °C for 2 h before thermogravimetric and differential thermal analyses were conducted to explore its thermal stability [32,33]. As shown in Figure 1a, there is a mass loss of approximately 3% between room temperature and 800 °C, mostly attributed to the loss of absorbed matter and the dehydration of proton ceramics. Another obvious weight loss is observed between 800 and 1100 °C, which may possibly be associated with the non-stochiometric change of oxygen or lattice oxygen removal [34]. The specific surface area and pore size distribution analyses of the FeCo catalyst loaded onto the BZCYYb support are presented in Figure 1b; the FeCo/BZCYYb has a specific surface area of 23.92 m^2/g and a pore size of 5.43 nm. The use of BZCYYb as a support significantly increases the specific surface area of the catalyst, promoting the uniform dispersion of the FeCo catalyst particles and thereby enhancing the ammonia decomposition activity. The phase analyses of reduced monometallic Fe and Co and bimetallic Fe_mCo_n (which refers to Fe-Co at different molar ratios) catalysts were conducted via XRD, as shown in Figure 1c,d. After H_2 reduction, single-metal phases Fe and Co could be observed in the Fe/BZCYYb and Co/BZCYYb single-metal catalysts, respectively. The binary metals with varying doping ratios exhibited the presence of an FeCo alloy phase at $2\theta = 44.9°$, corresponding to the (110) crystal face[16,35], with the diffraction peak of BZCYYb remaining basically unchanged. Alloying can promote the activity of metal nanoparticles. The characteristic peak of $CoFe_2O_4$ was observed at $2\theta = 35°$ in the FeCo alloy phase (PDF: 00-003-0864), indicating that Co_3O_4 and Fe_2O_3 may form a composite metal oxide, $CoFe_2O_4$, when the catalyst remains un-reduced [36]. The XRD characteristic results are only qualitative due to the low active metal loading. Additionally, a trace $BaCO_3$ phase appeared at $2\theta = 34.7°$ in the XRD analysis, which may have been caused by the low calcined temperature during the pretreatment of the Ba precursor; however, a $BaCO_3$ phase did not appear when calcining to 1100 °C during the BZCYYb precursor treatment. Importantly, NH_3 decomposition tests show that the $BaCO_3$ phase does not affect the catalytic activity of the catalyst.

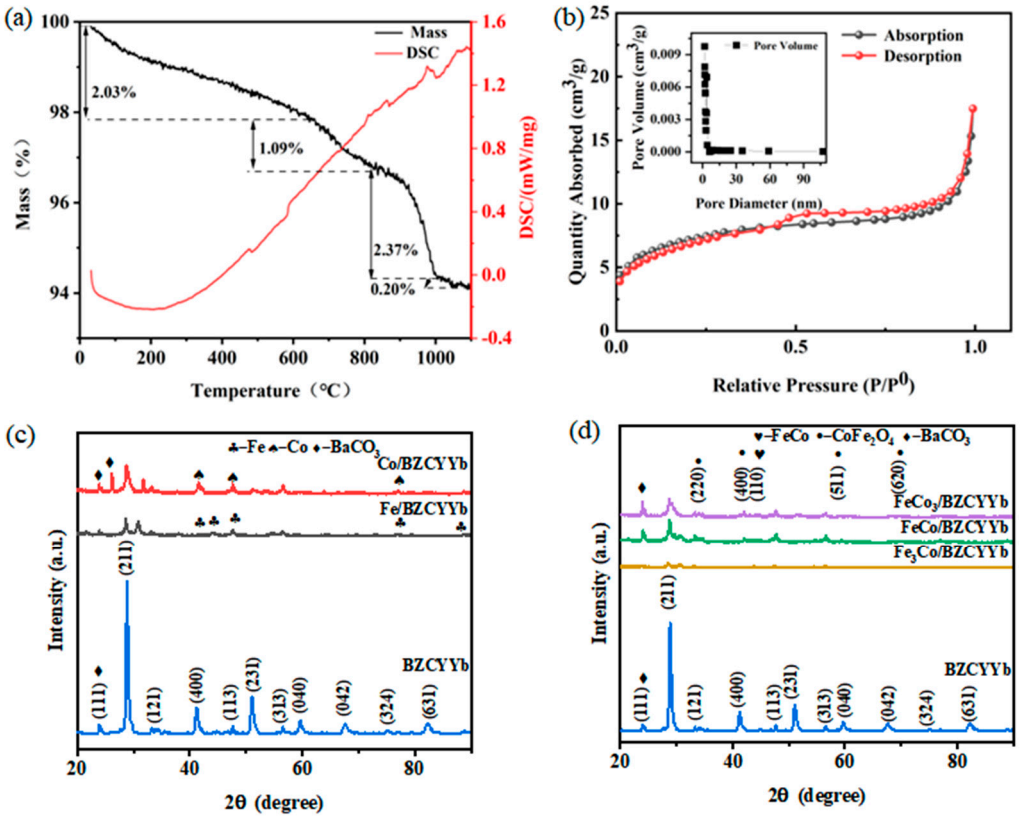

Figure 1. (**a**) TG-DSC curves of BZCYYb support pre-calcined at 1000 °C for 2 h within the temperature range of 30–1100 °C. (**b**) Specific surface area and pore size distribution of FeCo bimetallic catalysts supported on BZCYYb. XRD patterns of BZCYYb-supported samples: (**c**) monometallic catalysts of Fe and Co; (**d**) different rations of Fe_mCo_n bimetallic catalysts.

Figure 2 illustrates the microstructure and EDS mapping of reduced bimetallic catalysts and the BZCYYb support. As shown in Figure 2a–c, the dissolution of catalyst particles on the surface of the BZCYYb indicates that catalyst particles have been effectively loaded onto the support without visible particle agglomeration, and that the active metals Fe and Co are uniformly distributed on the support. The presence of surface pore structures ensures sufficient contact with the fuel gas, thereby promoting efficient interactions between the fuel and active sites, promoting catalytic activity over a larger surface area. Figure 2m–r show the TEM analysis of the FeCo/BZCYYb catalyst after it has been thoroughly dispersed in ethanol and ultrasonicated before the TEM operation. Nanosized clusters likely to be the catalysts can be observed. Since the support was relatively thick when compared to the nano clusters, we were unable to directly obtain a diffraction pattern for the cluster's crystal structure. However, it can be seen through the EDS mapping spectra that the Fe catalyst particles are uniformly distributed on the support, and Co appears to be locally agglomerated, but macroscopically uniformly distributed.

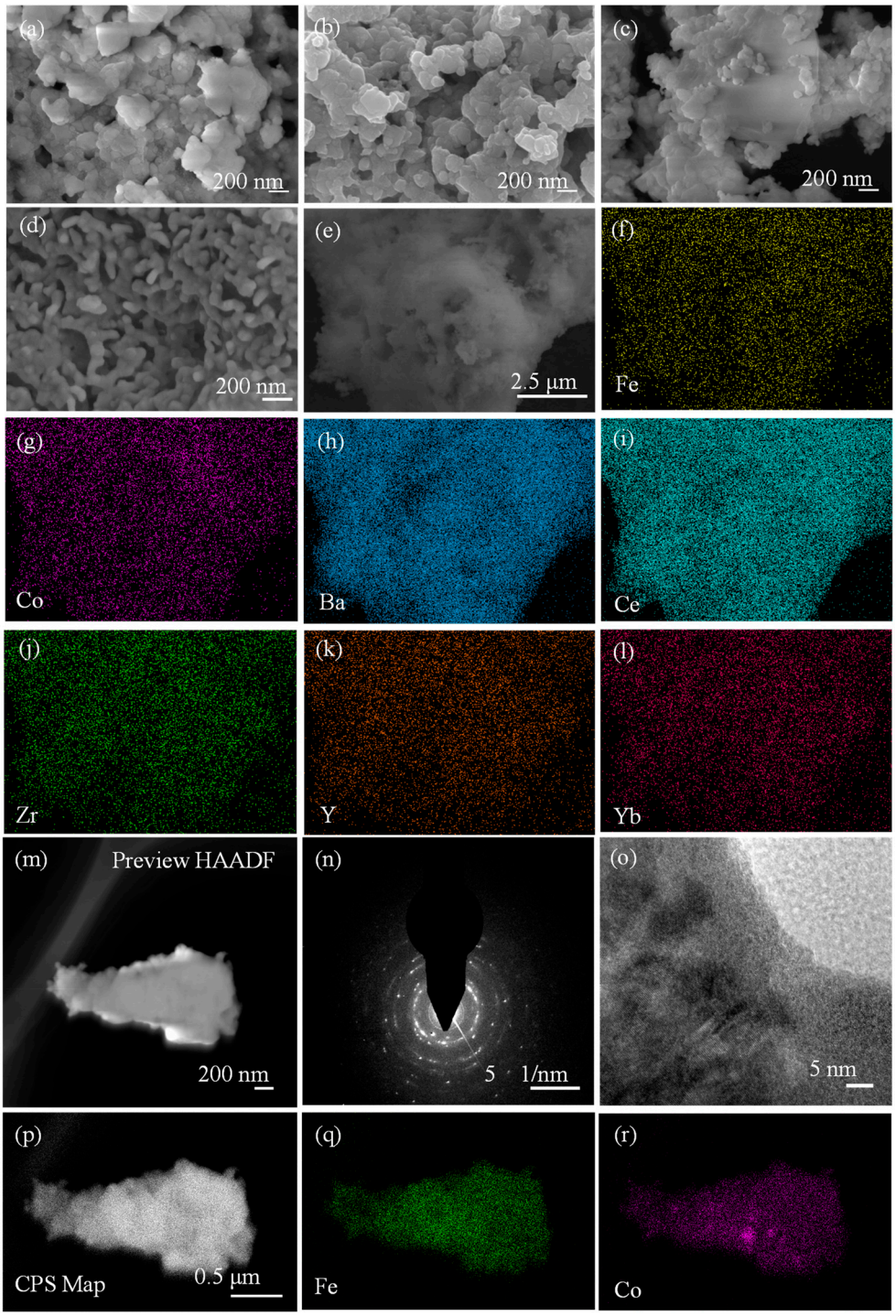

Figure 2. SEM images and EDS mapping of reduced bimetallic catalysts: (**a**) Fe_3Co/BZCYYb; (**b**) FeCo/BZCYYb; (**c**) $FeCo_3$/BZCYYb; (**d**) BZCYYb; (**e**) electron image of FeCo/BZCYYb; (**f**) Fe; (**g**) Co; (**h**) Ba; (**i**) Ce; (**j**) Zr; (**k**) Y; (**l**) Yb. HRTEM images of FeCo/BZCYYb: (**m–o**). CPS mapping of FeCo/BZCYYb: (**p**). EDS mapping images: (**q**) Fe; (**r**) Co.

As shown in Figure 3, XPS analysis was performed to investigate the electronic states and conduct a quantitative assessment of the active metals without support after H_2 reduction. This analysis revealed distinct peaks corresponding to metallic Fe 2p and Co 2p. In the Fe_3Co and FeCo bimetals, Fe metallic peaks were observed at 706.7–708 eV, indicating the presence of metallic Fe in the reduced bimetallic catalyst. The XPS spectral fraction of Fe 2p was fitted by four deconvolution peaks: the Fe^{2+} $2p_{3/2}$ peak at 710.3–710.6 eV, the Fe^{0} $2p_{1/2}$ peak at 712.9–713.2 eV [25,37], and Fe^{3+} satellite peaks at about 719.2 eV,

with the Fe^{2+} satellite feature appearing at 716.47 eV in $FeCo_3$. For cobalt, metallic peaks were observed at 778–778.3 eV. The Co 2p spectra exhibited a Co^{3+} $2p_{3/2}$ peak at 779.8–780.3 eV and a Co^{2+} $2p_{3/2}$ peak at 781.8–782 eV, indicating the coexistence of Co^{2+} and Co^{3+} oxidation states [38]; Fe $2p_3/_2$ shifted from a higher oxidation state to a lower oxidation state, while Co shifted from a lower to a higher oxidation state. The Co $2p_{3/2}$ orbital shifted from a lower to a higher oxidation state as the Co/Fe ratio increased, leading to an increase in Co^{3+}/Co^{2+} content and a decrease in Fe^{3+} content [16]. XPS and XRD characterization indicated electron transfer between Co and Fe, suggesting the possible formation of an FeCo alloy phase on the surface during the reaction.

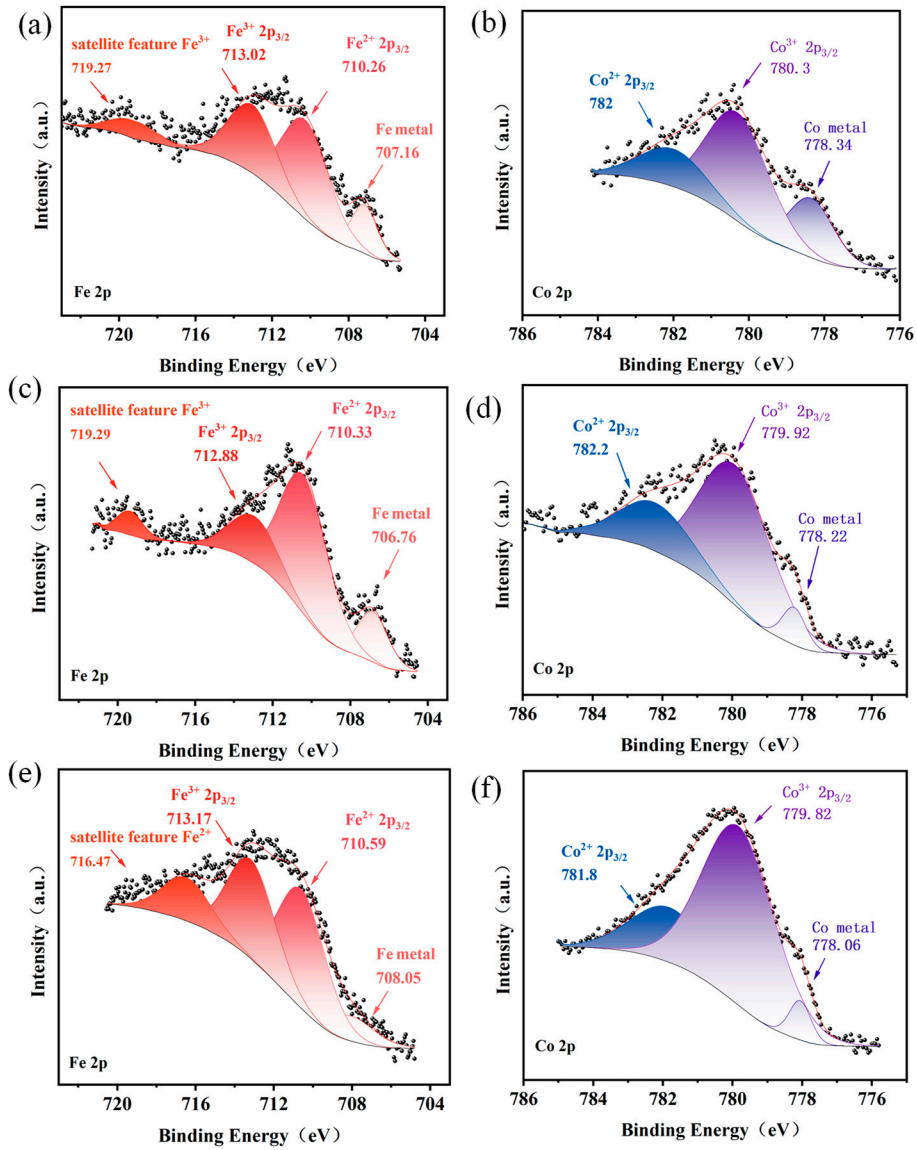

Figure 3. High-resolution XPS spectra of Fe 2p and Co 2p of bimetallic catalysts: (**a**,**b**) Fe_3Co; (**c**,**d**) FeCo; (**e**,**f**) $FeCo_3$.

The ammonia conversion of single-metal catalysts loaded onto BZCYYb as a function of the temperature are shown in Figure 4a. In the absence of catalysts, the ammonia decomposition efficiency in an empty quartz tube is relatively low, below 700 °C, and can be neglected. However, spontaneous decomposition occurs between 750 °C and 800 °C, with a conversion of 53.9% at 800 °C. The ammonia conversion of the catalyst increases with increasing temperature, as can be expected. At low and medium temperatures, the ammonia conversion rates of Co-based and Ni-based catalysts are higher; the ammonia

conversion of Fe-based catalysts varies greatly with temperature, while the ammonia conversion of Mn-based and Cu-based catalysts is lower at 650 °C, at 18.2% and 19.4%, respectively, which is consistent with the "volcano curve" [39]. This "volcano curve", combined with the fact that the cost of Fe is much lower than the costs of Co and Ni, indicates that the selection of Fe-based binary alloy catalysts is preferred. In particular, we would recommend an Fe-Co alloy over an Fe-Ni alloy due to the slightly better performance of Co at lower temperatures. As shown in Figure 4b, the ammonia conversion of catalysts with different Fe-Co molar ratios increases continuously with the increasing testing temperature. Co doping significantly changes the catalytic performance compared with a pure Fe catalyst: the ammonia decomposition performance of the bimetallic catalysts becomes substantially improved, with the ammonia conversion rates of the catalysts all reaching 100% within the ammonia detector's accuracy at 600 °C after doping with Co. The ammonia conversion fraction increases with the increase in Co content in the catalyst. Ammonia conversion is increased by 21.8% at an Fe-Co molar ratio of 5/5 compared to pure Fe. It can be seen that the Fe-Co molar ratio has a significant effect on the activity of catalysts for ammonia decomposition. In order to compare the effect of the support on the bimetallic catalyst according to the ammonia conversion fraction, we also studied FeCo catalysts on other types of support, namely ATP, Al_2O_3, and 3YSZ, as shown in Figure 4c. At 600 °C, the ammonia conversion fractions for ATP, Al_2O_3, and 3YSZ are 71%, 82.1%, and 88.8%, respectively; with BZCYYb as the support, the FeCo catalyst exhibits superior activity, possibly attributed to enhanced synergistic effects facilitated by the BZCYYb support [40].

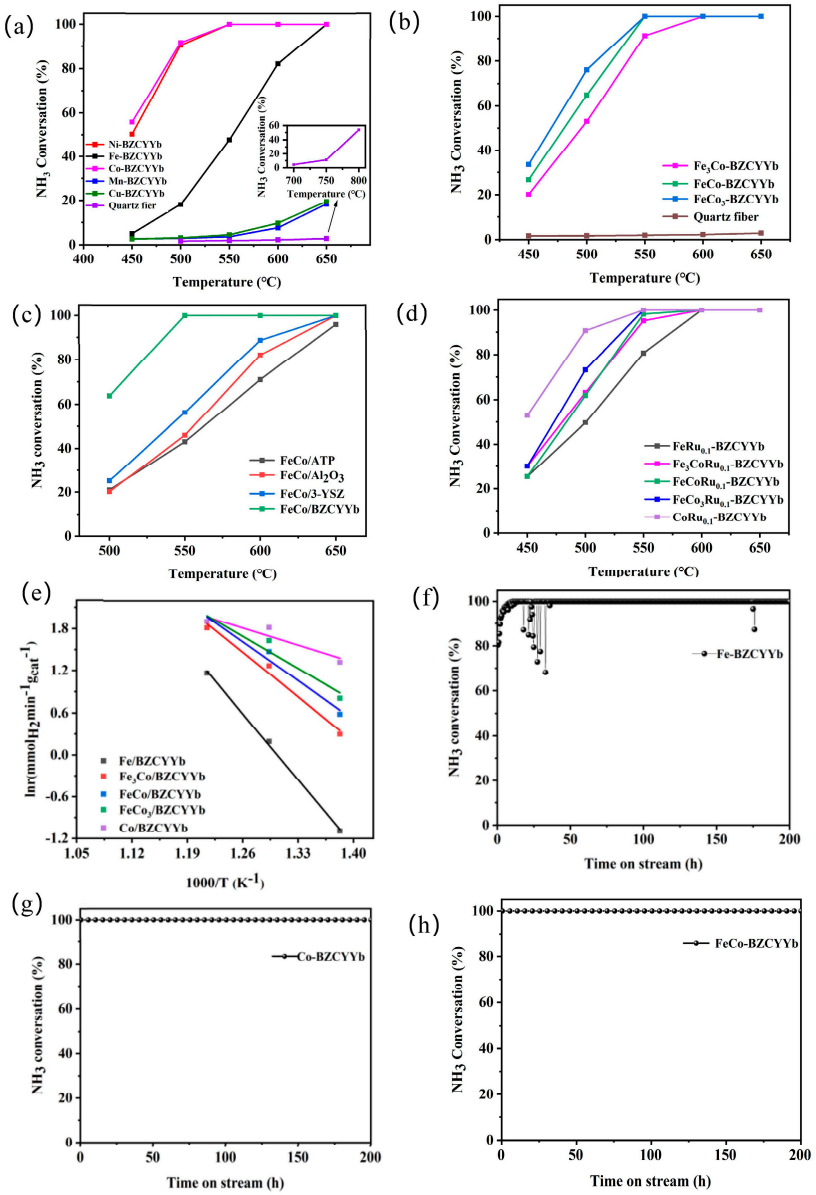

Figure 4. Ammonia decomposition activity of (**a**) monometallic catalysts of Fe, Co, Ni, Mn, and Cu; (**b**) bimetallic catalysts of different rations of Fe_mCo_n supported on BZCYYb; (**c**) FeCo active metals loaded onto different supports; (**d**) different rations of Fe_mCo_n with 0.1 wt.% Ru trimetallic catalysts supported on BZCYYb; and (**e**) the relationship between the ammonia decomposition rate of monometallic and bimetallic catalysts and the reaction temperature. The stability of catalysts for ammonia conversation at 600 °C with a GHSV of 6000 L $Kg^{-1}h^{-1}$: (**f**) Fe/BZCYYb; (**g**) Co/BZCYYb; and (**h**) FeCo/BZCYYb.

Since Ru at greater than 1 wt.% has been commonly used for ammonia decomposition [41,42], we also studied the effects of trace doping of Ru on top of non-precious metals to see if the introduction of a small amount of Ru, i.e., 0.1 wt.%, could further boost the catalytical performance. Figure 4d shows the ammonia decomposition fraction of Fe_mCo_n catalysts doped with 0.1 wt.% Ru at various ratios. After the doping with trace amounts of Ru, the ammonia conversion of the $FeRu_{0.1}$/BZCYYb catalyst increases significantly, and a slight increase in ammonia conversion is observed in $Fe_3CoRu_{0.1}$/BZCYYb catalyst. However, as the Co content increases, the ammonia conversion fractions of $FeCoRu_{0.1}$/BZCYYb, $FeCo_3Ru_{0.1}$/BZCYYb, and $CoRu_{0.1}$/BZCYYb remain constant or even decrease within the temperature range of 450–550 °C. This may be attributed to the interaction between Ru and Co, which modifies the electronic structure

and reduces the activity of the metal active sites, thereby impairing their ability to adsorb ammonia molecules, negatively affecting the efficiency of ammonia decomposition. Therefore, on one hand, the introduction of a trace amount of Ru seems unnecessary for Fe_mCo_n bimetallic catalysts. One the other hand, this may imply that the Fe-Co bimetallic catalysts on a BZCYYb support may already be sufficiently good.

On the basis of the experimental data, the kinetics of ammonia decomposition over the catalysts, expressed in terms of the H_2 generation rate, was also investigated. According to the material balance of the plug flow reactor and the calculation procedure discussed elsewhere [43], the apparent activation energy, E_a, of the ammonia decomposition reaction under different catalyst conditions was determined and compared with other reported studies, as shown in Table 1. The apparent activation energy of Fe/BZCYYb, Co/BZCYYb, and FeCo/BZCYYb are, respectively, 111.81, 51.92, and 96.23 kJ mol^{-1}. The decreasing trend of the apparent activation energy is almost in line with the amount of Co doping, which is consistent with the ammonia decomposition rate of each catalyst in Figure 4a,b. The Fe-based catalysts having the highest activation barrier may be related to the high coverage of N on the reconstructed surface due to the strong binding effect of Fe on N. It is well known that the recombination desorption of surface N atoms is the rate-limiting step in the ammonia decomposition reaction [32]. Co has one more d-band electron than Fe, so the formation of FeCo on the surface results in the transfer of electrons to Fe; this change in the electronic properties of Fe facilitates the desorption of adsorbed N atoms from the surface, thus reducing the activation barrier for the ammonia decomposition reaction. The Fe/BZCYYb catalyst showed the highest activation energy, while the $FeCo_3$/BZCYYb catalyst exhibited high activity and the lowest activation energy, suggesting that bimetallic FeCo catalysts can increase the apparent activation energy when compared to monometallic Fe catalysts.

Table 1. Catalytic activity of monometallic and bimetallic ammonia decomposition catalysts.

Catalyst	Metal Loading (wt.%)	Temperature (°C)	GHSV (mL $h^{-1}g^{-1}$)	Conversion (%)	Apparent Activation Energy (kJ mol^{-1})	Ref.
Fe/CNTs	5	500	6000	15	142	[44]
Fe/Al_2O_3	90	600	36,000	86	127	[45]
Fe/La-MgO	20	400	22,000	3	197	[46]
Fe/BZCYYb	10	550	6000	47.7	111.81	This work
Co/CNTs	7	450	5200	8	93	[47]
Co/La-MgO	20	400	22,000	37	167	[46]
Co/Y_2O_3	10	450	6000	28	-	[48]
Co/BZCYYb	10	450	6000	55.8	51.92	This work
Ni/SiO_2-Al_2O_3	65	450	30,000	9	92	[20]
Ni/Al_2O_3	20	500	7500	28	84	[49]
Ni/CeO_2-Al_2O_3	20	500	7500	53	70	[50]
Ni/La-MgO	20	400	22,000	28	182	[46]
Ni/SiO_2	10	550	36,000	50	108	[51]
Ru/ATP	1	500	6000	51	-	[52]
Ru/Ba-ZrO_2	3	500	30,000	24	92	[53]
Ru/Al_2O_3	4	450	125,000	33	95	[54]
Ru/B2CA	1	500	6000	100	-	[2]
Ru/CNTs	2.5	450	30,000	18	87	[55]
FeCo/CeO_2-S	5	550	36,000	75	125–148	[56]
FeCo/CNT	5	600	36,000	50	105	[16]
FeNi/SiO_2	10	550	14,400	24	71.1	[26]
$Fe_{8.3}Ni_{1.7}$/Al_2O_3	10	650	28,500	99.8	-	[57]

$FeCo/Al_2O_3$	10	350	36,000	82	-	[58]
$CoMo/SiO_2$	5	500	6000	20	82	[59]
Co_5Mo_8/Al_2O_3	13	527	30,000	60	106	[60]
$FeMo/Y_2O_3$-ZrO_2	10	550	46,000	16	-	[23]
$FeMo/La_2O_3$-Al_2O_3	10	550	46,000	50	-	[23]
$NiMo/SiO_2$	10	460	14,400	35.6	-	[61]
$Ni1Co_9$-CZY	10	550	48,000	63.7	41.1	[48]
NiCo/fumed SiO_2	10	550	30,000	76.8	54	[62]
Ni_2Fe_8/SiO_2	10	500	240,000	35	-	[21]
FeRu/CNTs	1.7	450	6000	85	-	[63]
Ni_5Ru_1/CeO_2	6	450	15,000	86.1	124	[64]
$Ru_3Fe/Al_2O_3/K$	4	400	5400	44	248	[7]
Cu_2Zn/CeO_2	18	550	15,000	53	79	[65]
Cu_2Zn/TiO_2	18	550	15,000	49	85	[65]
Fe_3Co/BZCYYb	10	550	6000	91.3	106.95	This work
FeCo/BZCYYb	10	500	6000	64.9	96.23	This work
$FeCo_3$/BZCYYb	10	550	6000	100	82.88	This work

Notes: Ru/B2CA: $Ru/(BaO)_2(CaO)(Al_2O_3)$; $Ru_3Fe/Al_2O_3/K$:Al_2O_3 as support and K as promoter.

The long-term stability of monometallic and FeCo/BZCYYb catalysts for ammonia decomposition was evaluated at 600 °C and a GHSV of 6000 L $Kg^{-1}h^{-1}$, as shown in Figures 4f–h. During the 200 h test, the Fe-based catalyst showed an initial fluctuation in ammonia conversion and generally maintained a conversion of 100%; the Co-based catalyst displayed excellent stability, with almost no observable decline in performance. The FeCo/BZCYYb catalyst displayed no apparent performance deterioration over the 200 h duration, and, in comparison with Fe, this catalyst exhibited improved thermal stability significantly. This can be attributed to the formation of FeCo alloy nanoparticles, which inhibit atomic or grain migration to some extent, thus preventing substantial agglomeration and the emergence of metal nitrides, thereby confirming the long-term stability of the FeCo bimetallic catalyst.

We noticed in the above-mentioned results and within the capability of detector accuracy, ammonia conversion could reach 100%. Since a trace amount of ammonia is inevitable due to the thermodynamic equilibrium fact and the wide detecting range of the analyzer used, that is, 0–100%, we also performed gas chromatography measurements to more accurately verify the residual NH_3 concentration near the full conversion side. During the steady-state ammonia decomposition tests at 600 °C using FeCo/BZCYYb as the catalyst, the exhaust analysis indicated a residual ammonia volume fraction of 3.8%. Given that an acceptable error margin of approximately ±3% is permissible, the ammonia decomposition analyzer effectively reflects the variations in ammonia decomposition rates with temperature changes, thus confirming the excellent catalytic performance of the FeCo/BZCYYb catalyst in the medium to low temperature range.

As shown in Figure 5a–c, the bimetallic catalyst was characterized via SEM after ammonia decomposition tests at 450–650 °C. The morphology of the catalysts remained predominantly unchanged after the tests; however, some degree of agglomeration occurred, which became more pronounced with increasing Fe content. The XRD characterization presented in Figure 5d reveals that no metal nitride phase was formed. This result indicates that the incorporation of Co inhibits the formation of iron nitrides during the reaction with NH_3, thereby improving the catalyst's stability [66]. This observation is consistent with the findings from the previous long-term durability tests.

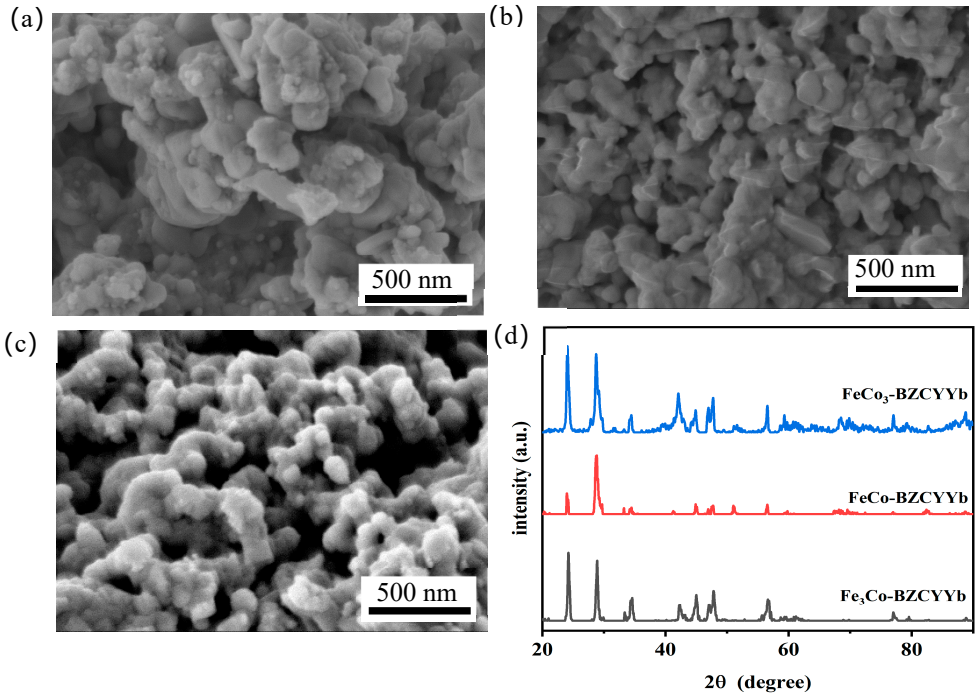

Figure 5. SEM images of bimetallic catalysts after ammonia decomposition tests: (**a**) Fe_3Co/BZCYYb, (**b**) FeCo/BZCYYb, and (**c**) $FeCo_3$/BZCYYb; (**d**) XRD pattern of bimetallic catalysts after ammonia decomposition tests.

One of the applications of ammonia decomposition catalysts is in external reforming on the anode side of fuel cells. It is necessary to point out that, at 600 °C, both the FeCo/BZCYYb and $FeCo_3$/BZCYYb catalysts achieved 100% ammonia decomposition rates. Given that Fe is a more affordable transition metal and exhibits good thermal stability over 200 h, we selected FeCo/BZCYYb as the catalyst for ammonia decomposition in SOFCs. To eliminate the effect of hydrogen partial pressure reduction in the ammonia decomposition gas, we introduced 100 mL/min 75% H_2 + 25% N_2 as fuel into the anode. As shown in Figure 6a, the peak power densities were 667.9 mW cm^{-2}, 555.9 mW cm^{-2}, and 420.8 mW cm^{-2} at 800 °C, 750 °C, and 700 °C, respectively. When using 50 mL/min cracked NH_3 as fuel, the corresponding peak power densities were 620.5 mW cm^{-2}, 508.2 mW cm^{-2}, and 374.6 mW cm^{-2} at 800 °C, 750 °C, and 700 °C, respectively. The performance of the cell running on cracked ammonia approached that observed with 75% H_2 + 25% N_2 as the fuel, though the performance remained slightly lower than that observed when using simulated fully converted gas of 75% H_2 + 25% N_2 by 7.09%, 8.58%, and 10.98% at 800 °C, 750 °C, and 700 °C, respectively. This may be attributed to the poisoning of trace NH_3 gas on the electro-catalytical surface.

Figure 6b,c show the impedance spectra of the tested cell with simulated fully converted gas and cracked NH_3 as fuel under open-circuit voltage. An analysis of the impedance spectra reveals that when using cracked NH_3 as fuel, the ohmic resistance (R_{ohmic}) slightly increases. Additionally, the difference between the two resistance values enlarges with decreasing temperature, possibly due to the adsorption of uncracked ammonia onto the electrolyte, which may damage its structural integrity [67]. Research by Zhu et al. indicates that no formation of Ni_3N could be detected following NH_3 fuel exposure based on element and phase characterization through TEM and XRD, as well as thermodynamic calculations. Furthermore, Ni_3N is unlikely to be the primary phase responsible for performance degradation [2]. However, the same study indeed observed profound morphological differences in nickel oxide particles between pure H_2 and NH_3 reduction. It is interesting to see that when cracked NH_3 serves as the fuel, the polarization

resistance (R_p) of the cells is lower than that observed with H_2; this phenomenon may be attributed to the catalytic action of Ni-based catalysts in the anode-promoting ammonia decomposition, which enhances the catalytic activity and improves the reactivity of the anode with H_2, thereby reducing polarization resistance.

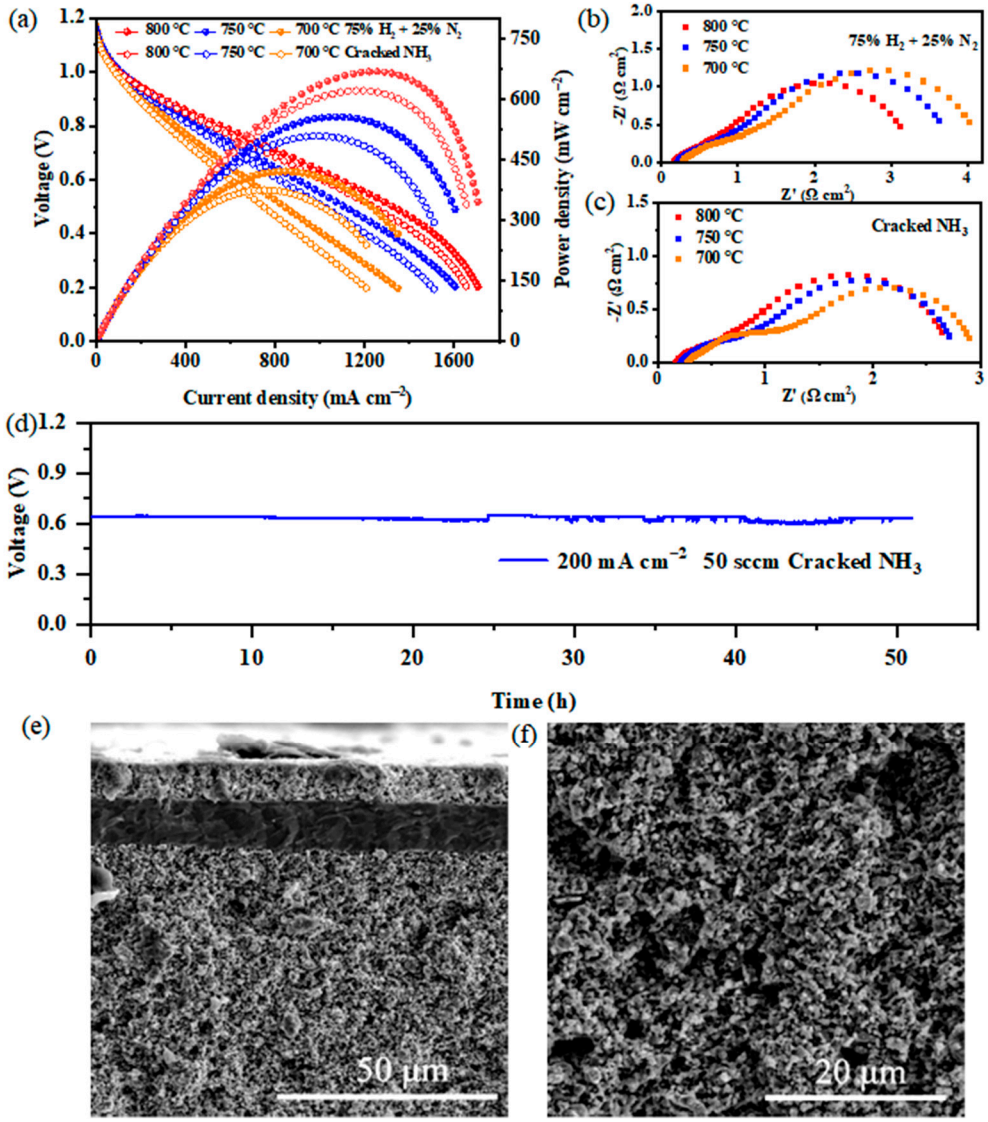

Figure 6. (**a**) Cell voltage and electrochemical performance of SOFCs operating with 75% H_2 + 25% N_2 and cracked NH_3 at various temperatures; (**b**,**c**) impedance spectra of SOFCs with 75% H_2 + 25% N_2 and cracked NH_3 at various temperatures, respectively; (**d**) short-term stability of SOFCs fed with cracked NH_3 operated at 700 °C and 200 mA cm^{-2}. SEM images of cells after a 50 h stability test with cracked NH_3: (**e**) cross-section of the cells, (**f**) anode surface of the cells.

The durability of the cells was tested using cracked NH_3 fuel operating at a temperature of 700 °C and a constant current of 200 mA cm^{-2}, as shown in Figure 6d, The results of the short-term stability tests show that the cells run stably with negligible degradation other than some small fluctuations, which may imply that some internal microstructural or interfacial changes have occurred. To verify this hypothesis, we conducted a postmortem analysis of the cells after the stability tests, as shown in Figure 6e,f. It can be observed that the cell structure is intact and the anode structure is porous. The electrolyte surface appears to be smooth, with no significant cracks and intergranular fractures can be seen at the interface between the anode and the electrolyte, indicating that

the catalyst provides an effective ammonia conversion, thus enabling the cell to maintain satisfactory electrochemical performance.

Based on the above analysis, the mechanism of FeCo catalysts facilitating ammonia decomposition reaction is summarized in Figure 7. NH_3 is initially adsorbed onto the active site of the metal catalyst, and the N-H bond is then broken and dehydrogenated to form metal–N compounds and adsorbed H species. As the H atoms continue to fall off, the adsorbed N atoms and H atoms finally recombine to form N_2 and H_2, whereas the electron transfer from the d-band of Co to Fe facilitates the desorption of the adsorbed N atoms on the surface and reduces the reaction barrier to increase the catalytic activity for the decomposition of ammonia [5,6,8]. The H_2 generated from the ammonia decomposition is passed into the anode of SOFCs, through the anode gas channel. Upon contact with the active surface of the three-phase interface, the O_2 at the cathode flows through the cathode channel, is adsorbed onto the surface of the cathode with catalytic reduction, and is then reduced to O^{2-}, which migrates to the anode through the electrolyte membrane to react with H_2 to generate H_2O and electrons.

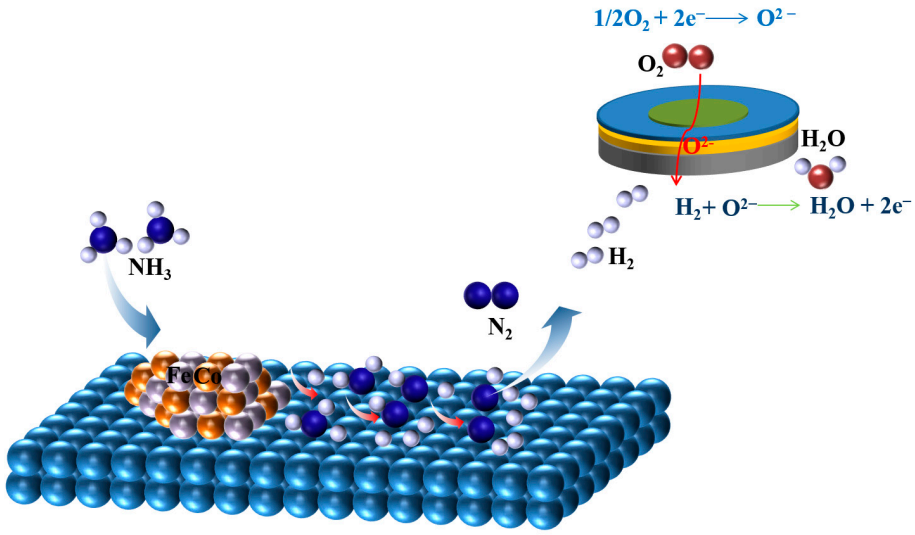

Figure 7. Schematic illustration of ammonia decomposition over FeCo/BZCYYb catalysts and the process of using externally reformed NH_3 as fuel for SOFCs.

3. Materials and Methods

3.1. Catalyst Preparation

The BZCYYb support, prepared using the sol–gel method (Ruier Powder Materials Corporation, Huizhou, China), was sintered at 1000 °C for 2 h to eliminate volatiles and enhance its thermal stability. $Fe(NO_3)_3{\cdot}9H_2O$ (Macklin Company, Shanghai, China), $Co(NO_3)_2{\cdot}6H_2O$ (Aladdin Company, Shanghai, China), $Ni(NO_3)_2{\cdot}6H_2O$ (Hushi Company, Shanghai, China), $Cu(NO_3)_2{\cdot}3H_2O$ (Aladdin Company), $Mn(NO_3)_2{\cdot}4H_2O$ (Aladdin Company), and $RuCl_3$ xH_2O (Aladdin Company) were used as metal precursors, which were impregnated into BZCYYb via the wet impregnation method; the catalyst preparation process is shown in Figure 8. The amounts of different metal precursors, including both non-precious metals and Ru used as control tests, and their designed loading contents are summarized in Table 2. In this study, we used Fe-decorated BZCYYb as an example to illustrate the process. Initially, $Fe(NO_3)_3{\cdot}9H_2O$ of an amount corresponding to 0.1 g of Fe and 0.9 g of BZCYYb were dissolved in anhydrous ethanol separately and stirred to form a homogeneous solution and suspension, respectively, and then the two were mixed together to form a mixture. The mixture was subjected to 30 min of ultrasonic treatment to achieve uniform metal dispersion on the support, followed by

stirring in a fume hood until the ethanol completely evaporated. The resulting powder was then dried in an oven at 85 °C for 24 h and calcined at 600 °C for 2 h. Subsequently, it was reduced in situ at 600 °C for 3 h.

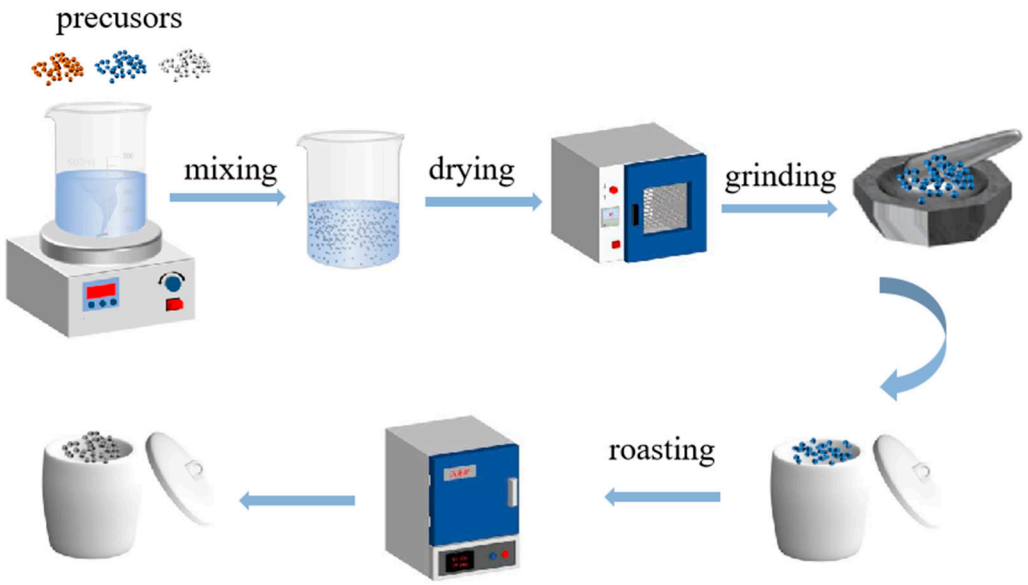

Figure 8. Depiction of Fe_mCo_n/BZCYYb catalysts synthesized via the wet impregnation method.

Table 2. Components of monometallic and bimetallic catalyst preparations.

Catalysts	$m_{active\ metal}$ (mg)	$n_{active\ metal}$ (mmol)	$m_{support}$ (mg)
Fe/BZCYYb	100	1.786	900
Co/BZCYYb	100	1.697	900
Ni/BZCYYb	100	1.704	900
Cu/BZCYYb	100	1.574	900
Mn/BZCYYb	100	1.820	900
Fe_3Co/BZCYYb	74:26:0	1.32:0.44	900
FeCo/BZCYYb	48.7:51.3	0.87:0.87	900
FeCo/ATP	48.7:51.3	0.87:0.87	900
$FeCo/Al_2O_3$	48.7:51.3	0.87:0.87	900
FeCo/YSZ	48.7:51.3	0.87:0.87	900
$FeCo_3$/BZCYYb	24:76:0	0.430:1.289	900
$FeRu_{0.1}$/BZCYYb	100:1	1.786:0.01	897.95
$Fe_3CoRu_{0.1}$/BZCYYb	74:26:1	1.32:0.44:0.01	897.95
$FeCoRu_{0.1}$/BZCYYb	48.7:51.3:1	0.87:0.87:0.01	897.95
$FeCo_3Ru_{0.1}$/BZCYYb	24:76:1	0.430:1.289:0.01	897.95
$CoRu_{0.1}$/BZCYYb	100:1	1.697:0.01	897.95

3.2. Catalyst Performance

To achieve hydrogen production from the ammonia decomposition, the catalytic activity of each catalyst was evaluated in a continuous fixed-bed quartz reactor. Briefly, a mixture of 0.1 g catalyst and 0.1 g quartz wool fiber was loaded into a quartz reactor, with additional quartz fiber at both ends of the quartz tube to ensure that the NH_3 was adequately heated and to capture any catalyst lost due to gas flow. Prior to the ammonia decomposition process, in situ reduction was performed by heating the catalysts in a N_2 atmosphere at a rate of 3 °C min^{-1} to 600 °C, followed by the introduction of 30 mL/min H_2 for 3 h to fully reduce the catalyst to its metallic state before increasing the temperature

to the test conditions. Pure ammonia was then introduced at a flow rate of 10 mL/min, achieving a GHSV of 6000 L Kg^{-1} h^{-1}. The ammonia conversion rate was determined using a calibrated ammonia decomposition rate analyzer (RL-B201, Runlai Instrument and Meter Co., Ltd., Xi'an, China) in the temperature range of 450–650 °C. While the NH_3 decomposition analyzer spans a full range, i.e., 0–100%, its accuracy near either 0 or 100% decomposition is insufficient when compared to that of a specially designed detector or analysis method for a given range, such as ppm-level detection for ammonia synthesis applications. In order to overcome and minimize the inevitable measurement errors involved in wide-range detection, the exhaust gas was collected from selected tests using bimetallic catalysts after thermal decomposition at 600 °C and used for gas chromatography analysis (Agilent 8890 GC-NCD, Agilent, Santa Clara, CA, USA) with nitrogen as a carrier gas and an injection port temperature of 250 °C in order to accurately quantify the residual NH_3 in the decomposition exhaust. The required data were recorded at the test temperature when a steady state was reached.

3.3. Fuel Cell Fabrication

The half-cell of an SOFC (Ningbo SOFCMAN Energy Technology Co., Ltd., Ningbo, China) has a structure of NiO-3YSZ|NiO-8YSZ|8YSZ. LSCF-GDC (Zhejiang H2-Bank Technology Co., Ltd., Ningbo, China) cathode slurry was applied to these half-cells using a screen-printing technique, and then sintering was performed at 950 °C for 2 h. The cells were sealed in an alumina tube using ceramic sealant (552-VFG, Aremco, Valley Cottage, NY, USA). A selected ammonia decomposition catalyst was mixed with quartz wool at a 1:1 weight ratio before being placed inside the previously mentioned fixed-bed quartz reactor; the off-gas from the reactor was then fed to the alumina tube of button cells as fuel. After reducing the cells at 800 °C for 1 h under a 75% H_2 + 25% N_2 gas mixture, electrochemical performance and impedance measurements were conducted at 700–800 °C.

3.4. Characterization

Mesoporous and BET analyses were conducted using an automatic specific surface area and porous analyzer (ASAP 2020 HD88, Micromeritics, Norcross, GA, USA) degassed at 200 °C in N_2 adsorption gas. Phase characterization was conducted via XRD (D8 DISCOVER XRD from BRUKER, Bremen, Germany). The X-ray source was Cu target K-α ray, the step size was 0.02°, and the scanning range was 10°~80°. The surface and particle size of the catalyst were observed using a field emission scanning electron microscope (FSEM, S4800, Hitachi, Tokyo, Japan) with a working voltage of 12 kV. Transmission electron microscopy (TEM) images and EDS mapping were accessed via TF20 (Tecnai F20, Tecnai, Hillsboro, OR, USA). Assessments of the chemical valence states and semi-quantitative analyses of the Fe and Co were performed using X-ray photoelectron spectroscopy (XPS, AXIS SUPRA, Kratos, Manchester, UK) with a Mg K radiation source.

4. Conclusions

In summary, this study investigates the ammonia decomposition activity of various single-metal and bimetallic non-precious metal catalysts over a proton-conducting ceramic support. Overall, our results reveal that the alloying of Fe with Co can significantly increase its conversion and stability and lower the overall cost of materials. The measured ammonia decomposition rate of FeCo/BZCYYb reached 100% at 600 °C. When BZCYYb was used as the support, the ammonia conversion rate achieved with the same loading of active metals was higher than that observed with other commonly used metal oxides as supports. This improvement may be attributed to the formation of an FeCo alloy, which facilitates electron transfer to Fe. The change in the electronic properties of Fe promotes the desorption of N atoms from the surface, thereby lowering the activation

energy barrier for the ammonia decomposition reaction. The FeCo/BZCYYb catalyst achieved 100% ammonia conversion at 600 °C within the measurement accuracy of the analyzer, and during a 200 h long-term stability test, the ammonia conversion remained at 100%. This indicates that FeCo/BZCYYb achieves excellent ammonia decomposition activity and long-term stability.

The catalyst was used in the production of hydrogen from ammonia decomposition for SOFCs. The performance of cells fed with cracked NH_3 was close to that achieved when using simulated fully converted gas with 75% H_2 + 25% N_2. A 50 h short-term test revealed that the cells could run stably with negligible degradation when using the cracked NH_3 as fuel. Future investigations may focus on integrating this catalyst into the anode of the cells to simplify the conversion process while maintaining high in situ conversion efficiency.

Author Contributions: X.Z.: methodology, investigation, formal analysis, writing—review and editing; Q.T., H.T., W.T., Y.C., J.S., and S.H.: investigation; B.Z. and W.G.: discussion and resources; H.L.: writing—review and editing; L.Z.: conceptualization, supervision, funding acquisition, writing—review and editing. All authors have read and agreed to the published version of the manuscript.

Funding: This work was supported by the Ningbo Municipal People's Government (Grant No. 2021A-162-G, Grant No. 2022Z027, Grant No. 2023Z103), and the Chinese Academy of Science.

Data Availability Statement: The data presented in this study are available.

Conflicts of Interest: The authors declare no conflicts of interest.

References

1. Afif, A.; Radenahmad, N.; Cheok, Q.; Shams, S.; Kim, J.H.; Azad, A.K. Ammonia-fed fuel cells: A comprehensive review. *Renew. Sustain. Energy Rev.* **2016**, *60*, 822–835.
2. Zhu, L.; Cadigan, C.; Duan, C.; Huang, J.; Bian, L.; Le, L.; Hernandez, C.H.; Avance, V.; O'Hayre, R.; Sullivan, N.P. Ammonia-fed reversible protonic ceramic fuel cells with Ru-based catalyst. *Commun. Chem.* **2021**, *4*, 121.
3. Chen, C.; Wu, K.; Ren, H.; Zhou, C.; Luo, Y.; Lin, L.; Au, C.; Jiang, L. Ru-Based Catalysts for Ammonia Decomposition: A Mini-Review. *Energy Fuels* **2021**, *35*, 11693–11706.
4. Chang, F.; Gao, W.; Guo, J.; Chen, P. Emerging Materials and Methods toward Ammonia-Based Energy Storage and Conversion. *Adv. Mater.* **2021**, *33*, e2005721.
5. Pan, Y.; Zhang, H.; Xu, K.; Zhou, Y.; Zhao, B.; Yuan, W.; Sasaki, K.; Choi, Y.; Chen, Y.; Liu, M. A high-performance and durable direct NH_3 tubular protonic ceramic fuel cell integrated with an internal catalyst layer. *Appl. Catal. B Environ.* **2022**, *306*, 121071.
6. He, F.; Gao, Q.; Liu, Z.; Yang, M.; Ran, R.; Yang, G.; Wang, W.; Zhou, W.; Shao, Z. A New Pd Doped Proton Conducting Perovskite Oxide with Multiple Functionalities for Efficient and Stable Power Generation from Ammonia at Reduced Temperatures. *Adv. Energy Mater.* **2021**, *11*, 2003916.
7. McCullough, K.; Chiang, P.-H.; Jimenez, J.D.; Lauterbach, J.A. Material Discovery and High Throughput Exploration of Ru Based Catalysts for Low Temperature Ammonia Decomposition. *Materials* **2020**, *13*, 1869.
8. Sun, S.; Jiang, Q.; Zhao, D.; Cao, T.; Sha, H.; Zhang, C.; Song, H.; Da, Z. Ammonia as hydrogen carrier: Advances in ammonia decomposition catalysts for promising hydrogen production. *Renew. Sustain. Energy Rev.* **2022**, *169*, 112918.
9. Thaker, A.; Mathew, M.; Hasib, N.; Herringer, N. A Review of Ammonia Fuel Cells. *Rev. Pap.* **2015**. https://doi.org/10.13140/RG.2.1.1700.7129
10. Fang, H.; Liu, D.; Luo, Y.; Zhou, Y.; Liang, S.; Wang, X.; Lin, B.; Jiang, L. Challenges and Opportunities of Ru-Based Catalysts toward the Synthesis and Utilization of Ammonia. *ACS Catal.* **2022**, *12*, 3938–3954.
11. Yin, S.F.; Xu, B.Q.; Zhu, W.X.; Ng, C.F.; Zhou, X.P.; Au, C.T. Carbon nanotubes-supported Ru catalyst for the generation of COx-free hydrogen from ammonia. *Catal. Today* **2004**, *93–95*, 27–38.
12. Ji, J.; Yan, X.; Qian, G.; Peng, C.; Duan, X.; Zhou, X. Morphology and location manipulation of Fe nanoparticles on carbon nanofibers as catalysts for ammonia decomposition to generate hydrogen. *Int. J. Hydrogen Energy* **2017**, *42*, 17466–17475.
13. Wang, W.; Fu, Y.; Wang, W.; Xiang, M.; Chen, G.; Su, Y.; Duan, J. Ammonia decomposition over La-doped Al_2O_3 supported Co catalyst. *Ceram. Int.* **2024**, *50*, 36604–36614.
14. Ogasawara, K.; Miyazaki, M.; Miyashita, K.; Abe, H.; Niwa, Y.; Sasase, M.; Kitano, M.; Hosono, H. Ammonia Decomposition over Water-Durable Hexagonal $BaTiO_{3-x}N_y$-Supported Ni Catalysts. *Adv. Energy Mater.* **2023**, *13*, 2301286.
15. Zhao, J.; Cui, C.; Wang, H.; Han, J.; Zhu, X.; Ge, Q. Insights into the Mechanism of Ammonia Decomposition on Molybdenum Nitrides Based on DFT Studies. *J. Phys. Chem. C* **2018**, *123*, 554–564.
16. Zhang, J.; Müller, J.-O.; Zheng, W.; Wang, D.; Su, D.; Schlögl, R. Weiqing. Individual Fe-Co Alloy Nanoparticles on Carbon Nanotubes: Structural and Catalytic Properties. *Nano Lett.* **2008**, *8*, 2738–2743.

17. Fu, E.; Qiu, Y.; Lu, H.; Wang, S.; Liu, L.; Feng, H.; Yang, Y.; Wu, Z.; Xie, Y.; Gong, F.; et al. Enhanced NH_3 decomposition for H_2 production over bimetallic M(M = Co, Fe, Cu)Ni/Al_2O_3. *Fuel Process. Technol.* **2021**, *221*, 106945.
18. Khan, W.U.; Alasiri, H.S.; Ali, S.A.; Hossain, M.M. Recent Advances in Bimetallic Catalysts for Hydrogen Production from Ammonia. *Chem. Rec.* **2022**, *22*, e202200030.
19. Lucentini, I.; Garcia, X.; Vendrell, X.; Llorca, J. Review of the Decomposition of Ammonia to Generate Hydrogen. *Ind. Eng. Chem. Res.* **2021**, *60*, 18560–18611.
20. Choudhary, T.V.; Sivadinarayana, C.; Goodman, D.W. Catalytic ammonia decomposition: CO_x-free hydrogen production for fuel cell applications. *Catal. Lett.* **2001**, *72*, 197–201.
21. Simonsen, S.B.; Chakraborty, D.; Chorkendorff, I.; Dahl, S. Alloyed Ni-Fe nanoparticles as catalysts for NH_3 decomposition. *Appl. Catal. A Gen.* **2012**, *447–448*, 22–31.
22. Yin, S.-F.; Zhang, Q.-H.; Xu, B.-Q.; Zhu, W.-X.; Ng, C.-F.; Au, C.-T. Investigation on the catalysis of COx-free hydrogen generation from ammonia. *J. Catal.* **2004**, *224*, 384–396.
23. Lorenzut, B.; Montini, T.; Bevilacqua, M.; Fornasiero, P. FeMo-based catalysts for H_2 production by NH_3 decomposition. *Appl. Catal. B Environ.* **2012**, *125*, 409–417.
24. Toulhoat, H.; Raybaud, P. Prediction of optimal catalysts for a given chemical reaction. *Catal. Sci. Technol.* **2020**, *10*, 2069–2081.
25. Zhang, S.; Han, M.; Shi, T.; Zhang, H.; Lin, Y.; Zheng, X.; Zheng, L.R.; Zhou, H.; Chen, C.; Zhang, Y.; et al. Atomically dispersed bimetallic Fe–Co electrocatalysts for green production of ammonia. *Nat. Sustain.* **2022**, *6*, 169–179.
26. Sun, S.-Q.; Yi, Y.-H.; Wang, L.; Zhang, J.-L.; Guo, H.-C. Preparation and Performance of Supported Bimetallic Catalysts for Hydrogen Production from Ammonia Decomposition by Plasma Catalysis. *Acta Phys.-Chim. Sin.* **2017**, *33*, 1123–1129.
27. Yang, l.; Wang, S.; Blinn, K. Enhanced Sulfur and Coking Tolerance of a Mixed Ion Conductor for SOFCs: $BaZr_{0.1}Ce_{0.7}Y_{0.2-x}Yb_xO_{3-6}$. *Science* **2009**, *326*, 126–129.
28. Duan, C.; Tong, J.; Shang, M.; Nikodemski, S.; Sanders, M.; Ricote, S.; Almansoori, A.; O'Hayre, R. Readily processed protonic ceramic fuel cells with high performance at low temperatures. *Science* **2015**, 349, 1321–1326.
29. Duan, C.; Kee, R.J.; Zhu, H.; Karakaya, C.; Chen, Y.; Ricote, S.; Jarry, A.; Crumlin, E.J.; Hook, D.; Braun, R.; et al. Highly durable, coking and sulfur tolerant, fuel-flexible protonic ceramic fuel cells. *Nature* **2018**, *557*, 217–222.
30. Xu, K.; Zhang, Y.Y.; Wang, W.W.; Peng, M.; Liu, J.C.; Ma, C.; Zhang, Y.W.; Jia, C.J.; Ma, D.; Yan, C.H. Single-atom Barium Promoter Enormously Enhanced Non-noble Metal Catalyst for Ammonia Decomposition. *Angew. Chem. Int. Ed. Engl.* **2024**, e202416195.
31. Yin, S.F.; Xu, B.Q.; Zhou, X.P.; Au, C.T. A mini-review on ammonia decomposition catalysts for on-site generation of hydrogen for fuel cell applications. *Appl. Catal. A Gen.* **2004**, *277*, 1–9.
32. Mukherjee, S.; Devaguptapu, S.V.; Sviripa, A.; Lund, C.R.F.; Wu, G. Low-temperature ammonia decomposition catalysts for hydrogen generation. *Appl. Catal. B Environ.* **2018**, *226*, 162–181.
33. Xun, Y.; He, X.; Yan, H.; Gao, Z.; Jin, Z.; Jia, C. Fe- and Co-doped lanthanum oxides catalysts for ammonia decomposition: Structure and catalytic performances. *J. Rare Earths* **2017**, *35*, 15–23.
34. Xia, L.-N.; He, Z.-P.; Huang, X.W.; Yu, Y. Synthesis and properties of $SmBaCo_{2-x}Ni_xO_{5+\delta}$ perovskite oxide for IT-SOFC cathodes. *Ceram. Int.* **2016**, *42*, 1272–1280.
35. Lendzion-Bieluń, Z.; Pelka, R.; Czekajło, Ł. Characterization of FeCo based catalyst for ammonia decomposition. The effect of potassium oxide. *Chem. Technol.* **2014**, *16*, 111–116.
36. Alves, T.E.P.; Pessoni, H.V.S.; Franco, A.; Burda, C.; Samia, A.C.S. Magnetic-plasmonic properties of $CoFe_2O_4$@Au nanocomposite. *J. Phys. Chem. Solids* **2022**, *164*, 110630.
37. Li, T.; Zhao, S.; Lu, Y.; Li, Z.; Gao, Z.-D.; Song, Y.-Y. An anion exchange reaction: An effective approach to prepare alloyed Co–Fe bimetallic disulfide for improving the electrocatalytic activity. *Chem. Commun.* **2019**, *55*, 7615–7618.
38. Zhong, M.; Yang, D.H.; Kong, L.J.; Shuang, W.; Zhang, Y.H.; Bu, X.H. Bimetallic metal-organic framework derived Co_3O_4-$CoFe_2O_4$ composites with different Fe/Co molar ratios as anode materials for lithium ion batteries. *Dalton Trans.* **2017**, *46*, 15947–15953.
39. Bell, T.E.; Torrente-Murciano, L. H_2 Production via Ammonia Decomposition Using Non-Noble Metal Catalysts: A Review. *Top. Catal.* **2016**, *59*, 1438–1457.
40. Wang, L.; Yi, Y.; Zhao, Y.; Zhang, R.; Zhang, J.; Guo, H. NH_3 Decomposition for H_2 Generation: Effects of Cheap Metals and Supports on Plasma–Catalyst Synergy. *ACS Catal.* **2015**, *5*, 4167–4174.
41. Hu, X.-C.; Fu, X.-P.; Wang, W.-W.; Wang, X.; Wu, K.; Si, R.; Ma, C.; Jia, C.-J.; Yan, C.-H. Ceria-supported ruthenium clusters transforming from isolated single atoms for hydrogen production via decomposition of ammonia. *Appl. Catal. B Environ.* **2020**, *268*, 118424.
42. Chung, D.B.; Kim, H.Y.; Jeon, M.; Lee, D.H.; Park, H.S.; Choi, S.H.; Nam, S.W.; Jang, S.C.; Park, J.-H.; Lee, K.-Y.; et al. Enhanced ammonia dehydrogenation over Ru/La(x)-Al_2O_3 (x = 0–50 mol%): Structural and electronic effects of La doping. *Int. J. Hydrogen Energy* **2017**, *42*, 1639–1647.
43. Yi Y.; Xu C.; Wang L.;Yu J.; Selectivity control of H_2/O_2 plasma reaction for direct synthesis of high purity H_2O_2 with desired concentration [J]. Chemical Engineering Journal, 2017, 313: 37-46.
44. Zhang, H.; Alhamed, Y. A.; Kojima, Y.; Al-Zahrani, A. A.;Petrov, L. A. Cobalt Supported on Carbon Nanotubes. An Efficient Catalyst for Ammonia Decomposition. C. R. Acad. Bulg. Sci. **2013**, 66(4), 519−524.

45. Gu, Y.-Q.; Jin, Z.; Zhang, H.; Xu, R.-J.; Zheng, M.-J.; Guo, Y.-M.; Song, Q.-S.; Jia, C.-J. Transition metal nanoparticles dispersed in an alumina matrix as active and stable catalysts for COx-free hydrogen production from ammonia. *J. Mater. Chem. A* **2015**, *3*, 17172–17180.
46. Hu, X.-C.; Wang, W.-W.; Jin, Z.; Wang, X.; Si, R.; Jia, C.-J. Transition metal nanoparticles supported La-promoted MgO as catalysts for hydrogen production via catalytic decomposition of ammonia. *J. Energy Chem.* **2019**, *38*, 41–49.
47. Torrente-Murciano, L.; Hill, A.K.; Bell, T.E. Ammonia decomposition over cobalt/carbon catalysts—Effect of carbon support and electron donating promoter on activity. *Catal. Today* **2017**, *286*, 131–140.
48. Huang, C.; Li, H.; Yang, J.; Wang, C.; Hu, F.; Wang, X.; Lu, Z.-H.; Feng, G.; Zhang, R. $Ce_{0.6}Zr_{0.3}Y_{0.1}O_2$ solid solutions-supported Ni Co bimetal nanocatalysts for NH3 decomposition. *Appl. Surf. Sci.* **2019**, *478*, 708–716.
49. Vacharapong, P.; Arayawate, S.; Henpraserttae, S.; Katanyutanon, S.; Charojrochkul, S.; Lawtrakul, L.; Toochinda, P. Effect of Magnetic Inducement in Preparation of Ni/Ce-doped Al_2O_3 for Ammonia Decomposition. *ChemistrySelect* **2019**, *4*, 11913–11919.
50. Zhang, L.-F.; Li, M.; Ren, T.-Z.; Liu, X.; Yuan, Z.-Y. Ce-modified Ni nanoparticles encapsulated in SiO_2 for CO-free hydrogen production via ammonia decomposition. *Int. J. Hydrogen Energy* **2015**, *40*, 2648–2656.
51. Atsumi, R.; Noda, R.; Takagi, H.; Vecchione, L.; Di Carlo, A.; Del Prete, Z.; Kuramoto, K. Ammonia decomposition activity over Ni/SiO_2 catalysts with different pore diameters. *Int. J. Hydrogen Energy* **2014**, *39*, 13954–13961.
52. Teng, Q.; Sang, J.; Chen, G.; Tao, H.; Wang, Y.; Li, H.; Guan, W.; Ding, C.; Liu, F.; Zhu, L. Ru/Attapulgite as an Efficient and Low-Cost Ammonia Decomposition Catalyst. *Catalysts* **2024**, *14*, 197.
53. Wang, Z.; Qu, Y.; Shen, X.; Cai, Z. Ruthenium catalyst supported on Ba modified ZrO_2 for ammonia decomposition to COx-free hydrogen. *Int. J. Hydrogen Energy* **2019**, *44*, 7300–7307.
54. Prasad, V.; Karim, A.M.; Arya, A.; Vlachos, D.G. Assessment of Overall Rate Expressions and Multiscale, Microkinetic Model Uniqueness via Experimental Data Injection: Ammonia Decomposition on $Ru/\gamma\text{-}Al_2O_3$ for Hydrogen Production. *Ind. Eng. Chem. Res.* **2009**, *48*, 5255–5265.
55. Wang, Z.; Cai, Z.; Wei, Z. Highly Active Ruthenium Catalyst Supported on Barium Hexaaluminate for Ammonia Decomposition to COx-Free Hydrogen. *ACS Sustain. Chem. Eng.* **2019**, *7*, 8226–8235.
56. Gao, Y.; Hu, E.; Yi, Y.; Yin, G.; Huang, Z. Plasma-assisted low temperature ammonia decomposition on 3d transition metal (Fe, Co and Ni) doped CeO_2 catalysts: Synergetic effect of morphology and co-doping. *Fuel Process. Technol.* **2023**, *244*, 107695.
57. Silva, H.; Nielsen, M.G.; Fiordaliso, E.M.; Damsgaard, C.D.; Gundlach, C.; Kasama, T.; Chorkendorff, I.b.; Chakraborty, D. Synthesis and characterization of $Fe–Ni/\gamma\text{-}Al_2O_3$ egg-shell catalyst for H_2 generation by ammonia decomposition. *Appl. Catal. A Gen.* **2015**, *505*, 548–556.
58. Akca, M.; Varisli, D. Performance of Co-Fe@Alumina catalysts in comparison to monometallic Co@Alumina and Fe@Alumina catalysts for microwave assisted COx-free hydrogen production. *Mol. Catal.* **2020**, *485*, 110823.
59. Ehiro, T.; Katagiri, K.; Yamaguchi, S.; Nishimura, T.; Saito, M.; Yoshioka, Y. The effects of the addition of calcium phosphate on catalytic activities for ammonia decomposition on CoMo-based catalysts. *J. Ceram. Soc. Jpn.* **2019**, *127*, 802–809.
60. Egawa, C. Ammonia Decomposition on Co/Mo(112) Model Surface. *e-J. Surf. Sci. Nanotechnol.* **2018**, *16*, 115–118.
61. Yi, Y.; Wang, L.; Guo, Y.; Sun, S.; Guo, H. Plasma-assisted ammonia decomposition over Fe–Ni alloy catalysts for COx-Free hydrogen. *AIChE J.* **2018**, *65*, 691–701.
62. Wu, Z.-W.; Li, X.; Qin, Y.-H.; Deng, L.; Wang, C.-W.; Jiang, X. Ammonia decomposition over SiO_2-supported Ni–Co bimetallic catalyst for COx-free hydrogen generation. *Int. J. Hydrogen Energy* **2020**, *45*, 15263–15269.
63. Chen, C.; Chen, Y.; Ali, A.M.; Luo, W.; Wen, J.; Zhang, L.; Zhang, H. Bimetallic Ru-Fe Nanoparticles Supported on Carbon Nanotubes for Ammonia Decomposition and Synthesis. *Chem. Eng. Technol.* **2020**, *43*, 719–730.
64. Lucentini, I.; García Colli, G.; Luzi, C.D.; Serrano, I.; Martínez, O.M.; Llorca, J. Catalytic ammonia decomposition over Ni-Ru supported on CeO_2 for hydrogen production: Effect of metal loading and kinetic analysis. *Appl. Catal. B Environ.* **2021**, *286*, 119896.
65. Dasireddy, V.D.B.C.; Hajduk, Š.; Ruiz-Zepeda, F.; Kovač, J.; Likozar, B.; Orel, Z.C. CeO_2 and TiO_2 support material effects on NH3 decomposition pathway mechanism over Cu–Zn catalysts. *Fuel Process. Technol.* **2021**, *215*, 106752.
66. Huang, X.; Lei, K.; Mi, Y.; Fang, W.; Li, X. Recent Progress on Hydrogen Production from Ammonia Decomposition: Technical Roadmap and Catalytic Mechanism. *Molecules* **2023**, *28*, 5245.
67. Meng, G.; Jiang, C.; Ma, J.; Ma, Q.; Liu, X. Comparative study on the performance of a SDC-based SOFC fueled by ammonia and hydrogen. *J. Power Sources* **2007**, *173*, 189–193.